

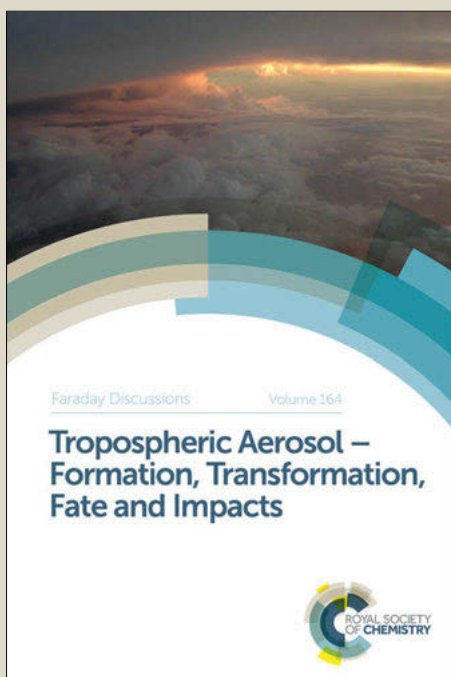
Faraday Discussions

Accepted Manuscript



This manuscript will be presented and discussed at a forthcoming Faraday Discussion meeting. All delegates can contribute to the discussion which will be included in the final volume.

Register now to attend! Full details of all upcoming meetings: <http://rsc.li/fd-upcoming-meetings>



This is an *Accepted Manuscript*, which has been through the Royal Society of Chemistry peer review process and has been accepted for publication.

Accepted Manuscripts are published online shortly after acceptance, before technical editing, formatting and proof reading. Using this free service, authors can make their results available to the community, in citable form, before we publish the edited article. We will replace this *Accepted Manuscript* with the edited and formatted *Advance Article* as soon as it is available.

You can find more information about *Accepted Manuscripts* in the [Information for Authors](#).

Please note that technical editing may introduce minor changes to the text and/or graphics, which may alter content. The journal's standard [Terms & Conditions](#) and the [Ethical guidelines](#) still apply. In no event shall the Royal Society of Chemistry be held responsible for any errors or omissions in this *Accepted Manuscript* or any consequences arising from the use of any information it contains.

Dry Mechanochemical Synthesis of Alane from LiH and AlCl₃

Ihor Z. Hlova,^{a,c} Shalabh Gupta,^{a*} Jennifer F. Goldston,^{a,b} Takeshi Kobayashi,^{a,b} Marek Pruski,^{a,b*} and Vitalij K. Pecharsky^{a,c*}

DOI: 10.1039/b000000x [DO NOT ALTER/DELETE THIS TEXT]

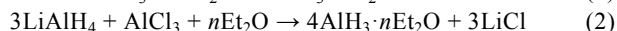
A mechanochemical process for the synthesis of alane (AlH₃) starting from lithium hydride (LiH) and aluminium chloride (AlCl₃) at room temperature and the underlying reaction pathway have been studied. In contrast to a conventional process using the same two reactants dissolved in diethyl ether, our approach enables a solvent-free synthesis, thereby directly leading to adduct-free alane. The method described here is quick and efficient, resulting in the quantitative conversion of all aluminium in the starting mixture to alane. Both the intermediate compounds formed during the reaction and the final products have been characterized by powder X-ray diffraction, solid-state ²⁷Al NMR spectroscopy, and temperature programmed desorption analysis of as-milled mixtures. We show that excess LiH in the starting mixture (with an optimal ratio of 9LiH:1AlCl₃) is essential for the formation and stability of Al-H bonds, initially in the form of alanates and, eventually, as alane. Further processing of this mixture, gradually adding AlCl₃ to reach the ideal 3LiH:1AlCl₃ stoichiometry, appears to restrict local accumulation of AlCl₃ during the ball-milling process, thereby preventing the formation of unstable intermediates that decompose to metallic Al and molecular hydrogen. We also demonstrate that under the milling conditions used, a moderate hydrogen pressure of ca. 300 bar is required to suppress competing reactions that lead to the formation of metallic Al at room temperature. Identification of the reaction intermediates at each stage of synthesis provides significant insight into the mechanism of this solid-state reaction, which may potentially afford a more rational approach toward the production of AlH₃ in a simple solvent-free process.

1. Introduction

The advantages of using hydrogen as an alternative to fossil fuels are manifold and well established, owing to its benign oxidation product (water) and gravimetric energy density that is up to three times that of gasoline.^{1,2} However, in order to enable transition to hydrogen fuel for consumer use, safe handling and transportation of hydrogen is of paramount concern. Solid-state hydrogen storage, in this regard, offers significant advantages over cryogenic and high-pressure approaches, since the safety risks associated with solid storage media are inherently lower than those posed by the latter options. Furthermore, solid materials also boast a significantly enhanced volumetric storage capacity relative to those typically encountered in cryogenic or high-pressure approaches. Despite these obvious advantages, however, more than five decades of research dedicated specifically to the development of materials-based hydrogen storage has led to only a few candidate materials that

exhibit performance parameters commensurate with requirements estimated for on-board vehicle applications. Of the materials identified, aluminium trihydride (AlH₃, also commonly known as alane) has attracted much interest due primarily to its excellent gravimetric and volumetric hydrogen capacities (10.1 wt% and 148 g/L, respectively)³ – both of which are theoretically compliant with the ultimate full fleet targets set by the U.S. Department of Energy (7.5 wt% and 70 g/L, respectively) to be achieved by 2017.⁴ In addition, AlH₃ completely dehydrogenates with an appreciable rate at temperatures close to 100 °C, which is an essential trait for compatibility with PEM fuel cells.⁵ Finally, AlH₃ releases pure hydrogen with only metallic Al remaining, the latter of which can be recycled relatively easily.

Notwithstanding its promising attributes, however, alane has not yet been widely utilized as a hydrogen storage material due mainly to the lack of a convenient process for its bulk synthesis. AlH₃ was first synthesized in 1942, as an amine complex.⁶ Later, Finholt *et al.* prepared an ethereal solution of AlH₃ by carrying out an exchange reaction between LiH and AlCl₃.⁷ It was not until 1955 that the non-solvated form of alane was reported, initially by Chizinsky *et al.*,⁸ and subsequently by Brower *et al.*⁹ via an organometallic route at the Dow Chemical Company. It was also discovered that AlH₃ could be synthesized from the hydrides or tetrahydroaluminates of alkali and alkaline earth metals via wet chemical processes,^{10–12} which usually involve the formation of alane-ether complexes such as those shown in Equations (1) and (2):⁷



Although at least seven polymorphic forms of AlH₃ have been discovered and characterized so far, only the α , α' , β and γ forms have been broadly studied, since these can be synthesized reproducibly and with quantitative yields.⁹ While all seven polymorphs decompose cleanly into the constituent elements, only the α -form does so in a single step (*i.e.*, without undergoing any phase transformation prior to the decomposition). Such a one-step desorption of hydrogen from a solid is an important material property from an engineering standpoint.

Based on thermodynamic considerations, the direct hydrogenation of metallic Al to form AlH₃ is highly unfavourable, and would hence require extremely high hydrogen pressures to proceed (in the range of a few GPa according to the phase diagram reported by Konovalov and Bulychev¹³). Although this has been achieved in a laboratory setting, such a process holds no merit for the large-scale production of AlH₃. In addition to the high-pressure solid-gas reaction, solvent-based processes have been developed, in which a range of organic amines are utilized as donor ligands to achieve direct hydrogenation of metallic Al under low hydrogen pressures.¹⁴ Aside from requiring large amounts of organic solvents, these approaches often only produce alane in the form of an adduct, which must then be subjected to purification processes often requiring ligand-exchange and heating, leading to significant decomposition of alane. Thus, novel procedures aimed at recycling metallic Al, albeit suitable only for off-board regeneration, are constantly sought to overcome the limitations of existing methods. Among those currently being explored, the electrochemical regeneration of aluminium hydride and the hydrogenation of metallic Al in supercritical fluids are notable.^{15,16}

Apart from the direct hydrogenation of metallic Al, the synthesis of AlH₃ from

LiAlH₄ and AlCl₃ has also been studied *via* alternative routes. Recent examples of adduct-free alane syntheses include the direct thermochemical conversion reported by Dinh *et al.*¹⁷, and several convenient, scalable, and energy-efficient mechanochemical methods developed by various groups.^{18–20} The solvent-free mechanochemical reaction between LiAlH₄ and AlCl₃ under ambient temperature conditions indeed leads to the production of AlH₃ (and LiCl), but not without suffering a net loss in hydrogen capacity from the formation of metallic Al, perhaps caused by the *in situ* thermal decomposition of nascent AlH₃ generated during the processing.^{18,19} One way to avoid this pitfall is to reduce the reaction temperature, preferably into the cryogenic range, but this would likely prove to be a complicated and expensive procedure during the scale-up.

Considering that LiAlH₄ is prepared either from LiH and AlCl₃ in diethyl ether,⁷ or through an ion-exchange reaction between NaAlH₄ and LiCl,²¹ it may be advantageous to be able to carry out a one-pot mechanochemical reaction starting from LiH. As far as we are aware, there is only one earlier report that describes the solid-state mechanochemical reaction between LiH and AlCl₃. According to the report, the mechanical agitation of a mixture with LiH:AlCl₃=3.6 for 4.5 h yielded only LiAlH₄ and LiCl with no evidence for the formation of alane.²² Herein, we report an efficient, room-temperature mechanochemical procedure for the synthesis of alane *via* a solid-state metathesis reaction between LiH and AlCl₃. The key element of this new strategy is adding one of the reagents, AlCl₃, in three discrete steps (rather than all at once) so as to direct the reaction pathway toward the desired product (AlH₃) and away from unstable intermediates. We also demonstrate that the gas pressure applied during mechanochemical processing may significantly affect the course of the reaction, which (to the best of our knowledge) has not hitherto been established.

2. Experimental

2.1. Materials and mechanochemical processing

LiH (Aldrich, 98 %) and AlCl₃ (Aldrich, 99.99 %) were used as starting materials without further purification. Because of the air and/or moisture sensitivity of the starting and the final compounds, all manipulations were performed in a continuously purified, argon-filled glove box with the oxygen and moisture levels controlled at less than 5 ppm (v/v). In a typical mechanochemical reaction, a total of ca. 1 g of starting material was weighed out in the desired molar ratio, and then transferred to a high-pressure stainless steel container that was filled with twenty chrome steel balls (11.9 mm dia.), each of which weighed ca. 7 g. The container was sealed under argon, and moved out of the glove box followed by evacuation and refilling with Zero grade H₂ (Linweld, 99.999%) until the desired pressure ranging between 1 to 350 bar was achieved. Ball-milling was carried out for various time intervals at 150 and 300 rpm with a ball-to-powder mass ratio (b:p) of ~140:1 in a two-station horizontal planetary mill (Fritsch, Pulverisette7). The milling sequence alternated between forward and reverse directions (2 min each) with an intermittent pause of 1 min to keep the average temperature of the vial as close to room temperature as possible during the entire ball-milling period (τ_{BM}).

2.2. X-ray powder diffraction analysis

Reaction products were characterized by X-ray powder diffraction (XRD) at room

temperature on a PANalytical X'PERT powder diffractometer using Cu $K_{\alpha 1}$ radiation with a 0.02° 2θ step, in the range of Bragg angles 2θ from 10° to 80° . In order to protect the samples from air and moisture the sample was covered by a thin polyimide (Kapton) film during the measurements. Presence of the film resulted in an amorphous-like background in the XRD patterns in the 2θ range of 13 – 20° .

2.3. Solid-state NMR spectroscopy

Common solid-state (SS)NMR parameters, which are referred to in the description below, are defined as follows: ν_{RF} is the magnitude of the applied radiofrequency (RF) field, t_{p} is the duration of the applied RF pulse, τ_{CP} is the contact time for cross polarization (CP), τ_{RD} is the relaxation delay between transients, NS is the number of transients collected for signal averaging, and ν_{R} is the magic angle spinning (MAS) rate.

All SSNMR data were collected on a 400-MHz (9.4 T) Agilent DD2 spectrometer equipped with a 3.2-mm Otsuka double resonance MAS probe using frequencies of 104.2 and 400.0 MHz for ^{27}Al and ^1H , respectively. ^{27}Al direct polarization (DP)MAS experiments were performed using single-pulse excitation under the following conditions: $\nu_{\text{R}} = 16$ kHz; $\nu_{\text{RF}}(^{27}\text{Al}) = 125$ kHz with $t_{\text{p}} = 0.2$ μs ; $\nu_{\text{RF}}(^1\text{H}) = 64$ kHz during two-pulse phase-modulation (TPPM) decoupling;²³ $\tau_{\text{RD}} = 1$ s; and NS = 512. Note that a short excitation pulse was employed in the DPMAS experiments to ensure that the observed signal intensities remained quantitative. The resulting numerical data obtained *via* integration of the relative signal intensities are given in the discussion below (represented as S_{DP}) as well as Table S1†. $^{27}\text{Al}\{^1\text{H}\}$ CPMAS experiments were collected under the following conditions: $\nu_{\text{R}} = 16$ kHz; $\nu_{\text{RF}}(^1\text{H}) = 100$ kHz during excitation (with $t_{\text{p}} = 2.5$ μs), and 64 kHz during CP and TPPM decoupling; $\nu_{\text{RF}}(^{27}\text{Al}) = \sim 48$ kHz during CP; $\tau_{\text{CP}} = 0.2$ ms; $\tau_{\text{RD}} = 60$ s; and NS = 512. All ^{27}Al spectra were referenced with respect to a 1.0 M aqueous solution of $\text{Al}(\text{NO}_3)_3$, which exhibits a single sharp resonance at 0 ppm.

Due to the sensitive nature of the materials involved in this study, all samples were packed within an argon-filled glove box using zirconia MAS rotors equipped with “gas-tight” accessories (*i.e.*, cap and spacer components that featured silicon rubber O-rings). These rotor accessories, when combined with careful packing protocols, were found to provide sufficient protection to the packed samples from air and/or moisture contamination, such that they could be removed from the glove box and analysed under ambient conditions, without spinning with dry nitrogen or using other precautionary measures (Fig S1†).

2.4. Temperature Programmed Desorption

Thermal desorption experiments were performed using a Setaram PCTPro-2000 automatic volumetric Sievert's type gas sorption instrument that was coupled to an RGA100 residual gas analyser. The as-prepared powder samples (ca. 0.15–0.2 g) were loaded in a custom built autoclave followed by volume calibration of the free sample space, which consisted of three helium absorption-desorption cycles over a period of 30–40 min. The thermal decomposition behaviour of the samples was studied by continuously monitoring the pressure change during heating at a rate of $4^\circ\text{C}/\text{min}$ from room temperature to 200°C . This was followed by soaking at this temperature until saturation was achieved. Qualitative analysis of the gases released during the experiment was performed after each measurement.

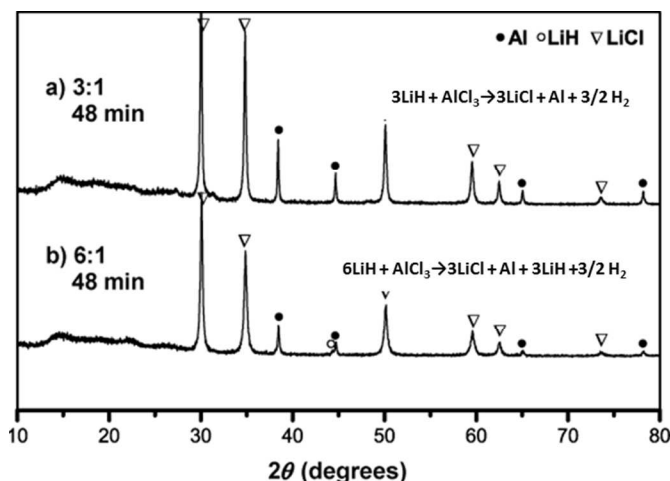


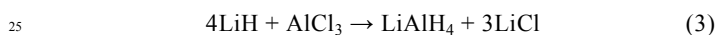
Fig. 1 X-ray diffraction patterns corresponding to as-milled samples with LiH:AlCl₃ starting ratios of a) 3:1, and b) 6:1, after ball-milling for 48 min under 350 bar H₂ with a milling speed of 300 rpm and a b:p of ~140.

3. Results and Discussion

In the following we first describe our efforts to optimize the synthetic conditions by analysing single-step reactions for different LiH:AlCl₃ ratios (3:1, 4:1, 6:1, 9:1 and 12:1) with hydrogen pressures between 1 and 350 bar. The lowest LiH:AlCl₃ ratio that did not result in accumulation of metallic Al (9:1) was then used to produce a series of samples for detailed spectroscopic examination and subsequent mechanochemical processing with additional AlCl₃ to yield AlH₃ and LiCl. We conclude by describing a series of follow-up experiments performed to refine the understanding of the reaction mechanisms.

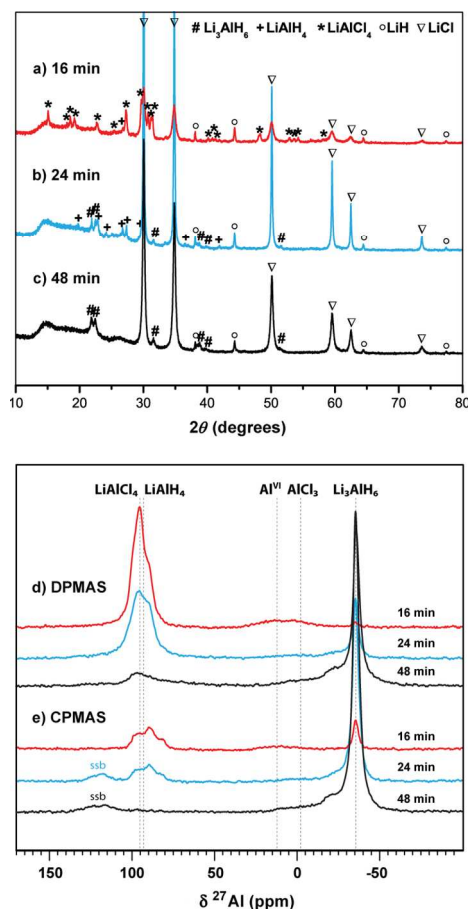
3.1 Determination of the initial reaction conditions

Based on the reported ethereal reaction between LiH and AlCl₃ (Eq. 1), a 3:1 molar mixture of LiH and AlCl₃ was prepared and processed mechanochemically under dry conditions (*i.e.*, in the absence of diethyl ether). After 48 min of processing at 300 rpm under 350 bar of H₂ pressure (the maximum hydrogen pressure rating of our vials) only metallic Al and LiCl were obtained as major products. The XRD pattern and the corresponding reaction are shown in Fig. 1a. Thereafter, an approach was attempted in which a slight excess of LiH (4LiH:1AlCl₃) was used to test whether the following reaction could provide a thermodynamically favorable pathway against the decomposition to metallic Al:



However, this attempt was also ineffective, yielding for $\tau_{\text{BM}} = 48$ min only metallic Al, LiCl, and unreacted LiH (XRD data not shown). Considering the very different reaction conditions presented by dry mechanochemical approach versus those encountered in solvent-based reactions, the failed attempts described above suggest that 1) the formation of alane-ether adducts in the solution-based approach is

essential for the stabilization of the hydride phase in (nearly) stoichiometric reactions, and 2) in each case, the reactions proceed *via* thermodynamically controlled pathways, which are distinct under such dissimilar conditions.



5 **Fig. 2** X-ray diffraction patterns (a-c) and SSNMR (^{27}Al DPMAS and $^{27}\text{Al}\{^1\text{H}\}$ CPMAS) spectra (d-
 e) obtained for samples of the 9:1 LiH:AlCl₃ reaction mass after ball-milling for the indicated time
 under 350 bar H₂ with a milling speed of 300 rpm and a b:p of ~140. Note that this reaction
 corresponds to the first stage of the stepwise mechanochemical synthesis of alane, as described in
 10 section 3.2. In the bottom two spectra of (e), 'ssb' is used to label a spinning sideband, which arises
 from the Li₃AlH₆ species.

We next hypothesized that the presence of a larger excess of hydride source in the
 starting mixture may prevent the formation of unstable intermediates that decompose
 to metallic Al. Indeed, when an arbitrarily chosen reaction mixture containing LiH
 15 and AlCl₃ in a molar ratio of 12:1 is processed under the same high hydrogen
 pressure, the reaction proceeds *without the formation of metallic Al*. Instead, lithium
 aluminium hexahydride (Li₃AlH₆), LiCl and unreacted LiH were obtained as the
 major products ($\tau_{\text{BM}} = 48\text{--}60$ min). Encouraged by these results, we set out to
 systematically explore the optimal composition of the starting mixture, and
 20 determined it to be 9LiH:1AlCl₃ under the milling parameters used. All reactions

carried out using LiH content less than this optimum resulted in metallic Al along with unreacted LiH, as shown in Fig. 1b for the starting mixture of 6:1. The processing of 9:1 mixture was also tested at lower pressures, and it was found that the minimum pressure required to avoid the formation of metallic Al is about 300 bar under the milling parameters used. Again, all reactions carried out at less than 300 bar lead to metallic Al, as well as LiCl and LiH (Fig. S2†).

3.2 The 9:1 reaction of LiH and AlCl₃ (stage 1)

To investigate further the results observed at the starting ratio of 9:1, the reaction mixture was sampled as a function of ball-milling time and the resulting products and intermediates were analysed by XRD in Fig. 2 (top panel) and SSNMR (bottom panel)—both of which provided clear and consistent mechanistic insight into the progression of the 9:1 reaction, as discussed below.

According to the XRD data obtained for $\tau_{\text{BM}} = 16$ min (pattern a), there exist three sets of Bragg peaks, including those from the reaction products, LiCl (the most intense peaks are at $2\theta \approx 30, 35, \text{ and } 50^\circ$)²⁴ and the monoclinic LiAlCl₄ (two sets of clearly identifiable Bragg peaks are at $2\theta \approx 15\text{--}20^\circ$ and $27\text{--}32^\circ$),^{25,26} as well as the unreacted LiH ($2\theta \approx 38$ and 44°).²⁷

SSNMR measurements revealed the presence of five Al-containing species at $\tau_{\text{BM}} = 16$ min. These include a small amount ($S_{\text{DP}} \cong 9\%$) of unreacted AlCl₃, represented in the ²⁷Al DPMAS spectrum by a broad peak centred around -2 ppm. (Note that AlCl₃ cannot be detected by ²⁷Al{¹H} CPMAS.) The dominant spectral band between 80 and 105 ppm ($S_{\text{DP}} \cong 84\%$) consists of two superimposed central transition powder patterns ascribed to LiAlH₄ and LiAlCl₄. The above assignments are based on the reference spectra of AlCl₃, LiAlH₄ and LiAlCl₄ in neat form shown in Fig. S3†. The relative contributions of LiAlH₄ and LiAlCl₄ are difficult to quantify due to severe spectral overlap. Indeed, the ²⁷Al quintuple-quantum (5Q)MAS measurements of neat LiAlH₄ and LiAlCl₄ materials have shown that the chemical shift and quadrupolar line shape parameters are very similar for these two species (Fig. S4†). Nonetheless, as noted several times in the ensuing discussion, useful information (*i.e.*, semi-quantitative approximations) can still be deduced from changes in the apparent lineshape of the superposition signal since the constituent powder patterns are known from the abovementioned reference spectra. Another hydride observed at this stage is Li₃AlH₆, represented by a peak near -35 ppm, which comprises only a minor fraction ($S_{\text{DP}} \cong 2\%$) of the quantitative DPMAS intensity but is featured quite prominently in the CPMAS spectrum. This highlights the selectivity associated with the CPMAS experiment, whereby ²⁷Al signals of species in close proximity to protons have the potential to be significantly amplified. By the same token, the absence of signals emanating from species such as AlCl₃ and LiAlCl₄ can be understood in terms of the lack of sufficiently nearby protons (*i.e.*, located within less than ~ 0.5 nm), without which ²⁷Al{¹H}CP cannot operate. Consequently, the only species observed *via* CPMAS in the present study are those containing protons (*i.e.*, various aluminium hydrides).

Finally, the broad, low-lying resonance occurring in the neighbourhood of 13 ppm in the DPMAS and CPMAS spectra presents a strong case for the presence of a small fraction ($S_{\text{DP}} \cong 5\%$) of six-coordinated Al^{VI} in AlH₃ and/or chloride-substituted AlCl_{3-x}H_x-type species that form at even earlier times.^{28,29} Indeed, it is quite possible that AlH₃ forms *via* the following reaction at early ball-milling times:

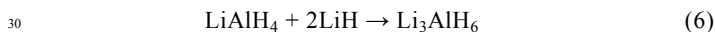


Equation 5a likewise supports the formation of LiAlCl_4 , which, according to both SSNMR and XRD analyses, also appears to be prominent at short milling times. Moreover, because the Al^{VI} hydrides are not observed near 13 ppm in later samples obtained for stage 1, they appear to exist only as transient intermediates, which quickly vanish upon further processing. (Note that such short-lived hydride intermediates are also observed in the SSNMR spectra corresponding to samples obtained early in stage 2.) One plausible explanation for the disappearance of these Al^{VI} intermediate hydrides is based on their transformation into LiAlH_4 , as shown for alane in the following reaction:³⁰



Thus, Eqs. 5a and 5b not only account for the initial formation of AlH_3 and its subsequent disappearance but are also consistent with the early preponderance of LiAlCl_4 and LiAlH_4 , directly in accord with SSNMR and XRD observations.

At $\tau_{\text{BM}} = 24$ min, the XRD pattern clearly shows the formation of LiAlH_4 ³¹ and Li_3AlH_6 ³² with a concomitant increase in LiCl and disappearance of the LiAlCl_4 phase (Fig. 2, pattern (b)). The corresponding DPMAS and CPMAS spectra (Fig. 2d,e, middle traces) confirm the presence of $\text{LiAlH}_4/\text{LiAlCl}_4$ ($S_{\text{DP}} \cong 73\%$). The peak centred at 95 ppm has now a lineshape that appears more characteristic of LiAlH_4 , suggesting that this species is largely responsible for the observed intensity at $\tau_{\text{BM}} = 24$ min. Accordingly, LiAlCl_4 is suspected to exist as only a minor component at 24 min. Also confirmed in the SSNMR spectra is the formation of Li_3AlH_6 ($S_{\text{DP}} \cong 24\%$) and the presence of unreacted AlCl_3 ($S_{\text{DP}} \cong 3\%$). Note that there is no indication of the aforementioned transient hydride species at 13 ppm. At this point, the relative abundance of Li_3AlH_6 can be explained by the following well-known transformation:³³



At $\tau_{\text{BM}} = 48$ min, the species detected by XRD were Li_3AlH_6 , LiCl and unreacted LiH (Fig. 2, pattern (c)). The corresponding SSNMR experiments revealed, as expected, an intense resonance from Li_3AlH_6 ($S_{\text{DP}} \cong 90\%$), and the apparent complete loss of LiAlH_4 . The minor resonance around 95 ppm ($S_{\text{DP}} \cong 10\%$) is assigned exclusively to LiAlCl_4 , as suggested by the absence of a CP signal. The disappearance of LiAlH_4 can likewise be understood on the basis of Eq. 6, with the complete consumption of this species signifying the end of stage 1. To ensure that this was the case, the milling time was extended up to 3 h and no significant change in the product profile was observed, thus providing further confirmation that the reaction is, indeed, complete at $\tau_{\text{BM}} = 48$ min under the milling conditions prescribed above.

With the exception of a few minor differences resulting mainly from the sensitivity of XRD only to the crystalline phases, and the detection of both crystalline and amorphous phases by SSNMR, both techniques provided consistent and complementary results describing in detail the overall mechanochemical transformation sequence for the reaction of $9\text{LiH}:1\text{AlCl}_3$ carried out at 350 bar H_2 pressure.

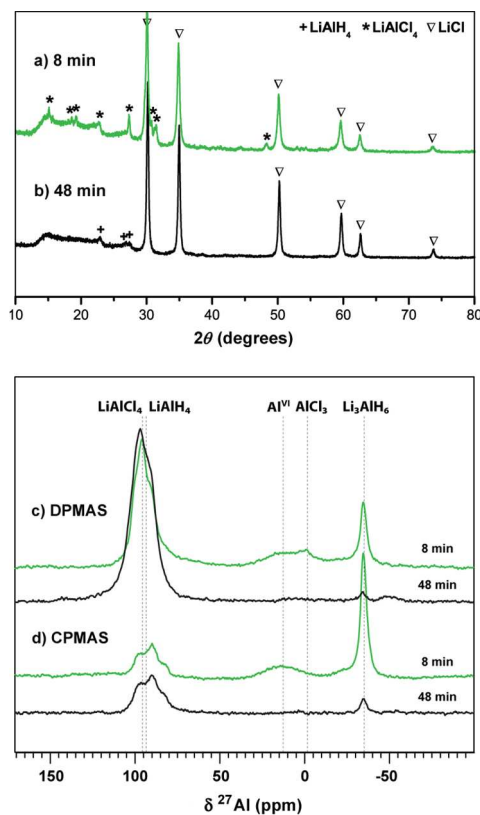


Fig. 3 X-ray diffraction patterns (a-b) and SSNMR (^{27}Al DPMAS and $^{27}\text{Al}\{^1\text{H}\}$ CPMAS) spectra (c-d) obtained for samples of the 4:1 LiH:AlCl₃ reaction mass after ball-milling for the indicated time under 350 bar H₂ with a milling speed of 300 rpm and a b:p of ~140. Note that this starting composition (obtained by adding 1.25 moles of AlCl₃ to the as-milled 9:1 products shown in Fig. 2) corresponds to the second stage of the stepwise mechanochemical synthesis of alane, as described in section 3.3.

3.3 Further addition of AlCl₃ (4:1 cumulative LiH:AlCl₃ ratio, stage 2)

Thereafter, 2 molar equivalents of AlCl₃ were added to the product mixture of stage 1 (Li₃AlH₆, LiCl and LiH at $\tau_{\text{BM}} = 48$ min) to reach the desired LiH:AlCl₃ ratio of 3:1. When the resulting mixture was processed under 350 bar of H₂ pressure, a dark grey powder was obtained after 15–20 min of ball-milling, indicating the formation of metallic Al, which was later confirmed by XRD analysis (not shown). However, when the amount of AlCl₃ added during the this first attempt was slightly reduced to 1.25 molar equivalents instead of 2 (resulting in an overall LiH:AlCl₃ ratio of 4:1 rather than 3:1), the reaction proceeded without the formation of metallic Al. Again, the progress of the reaction was monitored using XRD and SSNMR, the results of which are shown in Fig. 3 and described below.

For $\tau_{\text{BM}} = 8$ min, the XRD pattern shows only LiAlCl₄ and LiCl as the crystalline phases present in the sample. However, the ^{27}Al DPMAS spectrum of this sample shows signals at ~95, 13, -2, and -35 ppm representing LiAlH₄/LiAlCl₄ ($S_{\text{DP}} \cong 66\%$), six-coordinated Al^{VI} ($S_{\text{DP}} \cong 8\%$), AlCl₃ ($S_{\text{DP}} \cong 8\%$), and Li₃AlH₆ ($S_{\text{DP}} \cong 17\%$), respectively (Fig. 3, c-d for $\tau_{\text{BM}} = 8$). Although the relative contributions of LiAlH₄

and LiAlCl_4 are difficult to quantify, the lineshape of the superposition signal at 95 ppm is strikingly similar to that observed at $\tau_{\text{BM}} = 8$ min during stage 1, suggesting that the reactions occurring in each case are initiated by a similar mechanism, despite their overall stoichiometric differences. In addition, in both stages the spectra contain a similarly small, yet conspicuous, signal arising from Al^{VI} species around 13 ppm, which is absent at later processing times. Further still, these spectra also contain similar amounts of unreacted AlCl_3 at -2 ppm. In fact, apart from all of the similarities mentioned above, these spectra essentially differ only in the concentration of Li_3AlH_6 .

After $\tau_{\text{BM}} = 48$ min, the resonance observed at ~ 95 ppm dominates both the DPMAS ($S_{\text{DP}} \approx 97\%$) and CPMAS spectra. The lineshape of this resonance in the DPMAS spectrum indicates a larger contribution from LiAlH_4 , which is supported by a similar increase observed in the corresponding CPMAS signal. The only other species observed after 48 min of milling is Li_3AlH_6 , although it constitutes only $\sim 3\%$ of the overall DPMAS intensity. Thus, notwithstanding this and some relatively small fraction of LiAlCl_4 , the major product observed upon completion of stage 2 is LiAlH_4 , which is well in accord with Eq. 3 given the 4:1 ratio of $\text{LiH}:\text{AlCl}_3$ in the mixture.

3.4 Final addition of AlCl_3 (3:1 cumulative $\text{LiH}:\text{AlCl}_3$ ratio, stage 3)

Lastly, in order to obtain AlH_3 as the final product, another 0.75 molar equivalent of AlCl_3 was added to the mixture obtained upon completion of stage 2. The resulting mixture, having a net composition of $3\text{LiH}:\text{AlCl}_3$, was then processed as in the previous two stages. As was observed in stage 2 at $\tau_{\text{BM}} = 8$ min, the XRD pattern of the products at $\tau_{\text{BM}} = 10$ min shows only Bragg peaks corresponding to LiCl and LiAlCl_4 (Fig. 4, pattern (a)). It may be noted that the intensities for the LiAlCl_4 phase appear weak because of the relatively high concentration of LiCl in the sample. Although the expected Bragg peaks for AlH_3 are not observed in the diffraction patterns, together with the SSNMR results, the absence of metallic Al and the starting components indicate that the reaction proceeded as intended. Considering that the corresponding DPMAS spectrum exhibits a pronounced increase in the intensity of the signal at ~ 13 ppm assigned to the Al^{VI} species ($S_{\text{DP}} \approx 55\%$), the absence of Bragg peaks attributable to AlH_3 likely reflects the amorphous or nanocrystalline nature of the resulting aluminium trihydride. In addition to the resonance assigned to Al^{VI} , there is yet a substantial contribution from the signal occurring at ~ 95 ppm after 10 min, which encloses the remaining 45% of the total DPMAS intensity. Interestingly, the lineshape of this signal again closely resembles that observed at early points in the previous two stages. As such, it appears that comparable amounts of LiAlCl_4 and LiAlH_4 exist with the latter likely making a somewhat larger contribution. Regardless, it is quantitatively clear from the DPMAS spectrum that after 10 min of milling most of the aluminium species in the reaction mixture are now present as Al^{VI} hydrides.

At $\tau_{\text{BM}} = 48$ min, only the Bragg peaks corresponding to LiCl are observed by XRD. The corresponding SSNMR spectra now show only one resonance band centered around 13 ppm suggesting that all available Al has transformed to the hydrogenated Al^{VI} species. Note, however, that the line shape of the Al^{VI} signal in this sample differs slightly between the DPMAS and CPMAS experiments, suggesting that the final product may contain several polymorphic forms of AlH_3 or other structurally related species, most likely Cl-containing derivatives of AlH_3 ,

such as AlClH_2 ,^{28,29} though only in relatively small proportions.

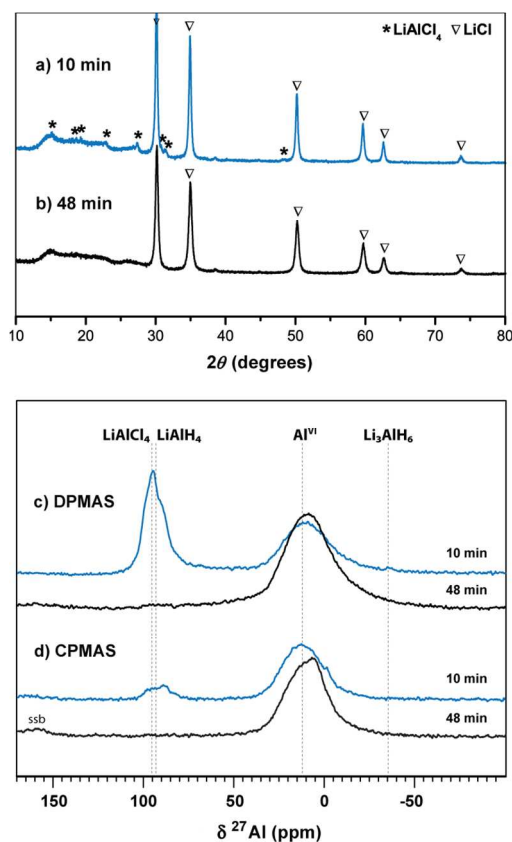
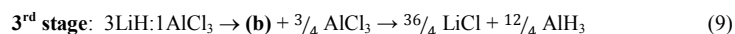
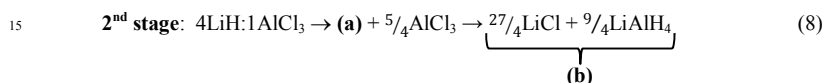
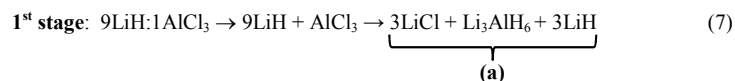


Fig. 4 X-ray diffraction patterns (a-b) and SSNMR (^{27}Al DPMAS and $^{27}\text{Al}\{^1\text{H}\}$ CPMAS) spectra (c-d) obtained for samples of the 3:1 LiH: AlCl_3 reaction mass after ball-milling for the indicated time under 350 bar H_2 with a milling speed of 300 rpm and a b:p of ~ 140 . Note that this starting composition (obtained by adding 0.75 moles of AlCl_3 to the as-milled 4:1 products shown in Fig. 3) corresponds to the third and final stage of the stepwise mechanochemical synthesis of alane, as described in section 3.4. In the last spectrum of (d), 'ssb' is used to label a spinning sideband, which arises from the Al^{VI} species.

3.5 Summary of the overall reaction scheme

Based on the XRD and SSNMR results, the reaction progress during stages 1–3 may be summarized as follows:



3.6 Temperature-programmed desorption (TPD) analysis

Further, the products that were obtained after completion of each stage, and their compositions were verified from the TPD curves. Figure 5 compares the decomposition profiles of products obtained from reactions 7–9 after $\tau_{\text{BM}} = 48$ min. The single-step desorption observed for the 9:1 sample (Fig. 5, curve (a)) has a desorption onset temperature (T_d) of ca. 180 °C, which is characteristic for the decomposition of pristine Li_3AlH_6 .^{34,35} The net hydrogen evolution of ca. 1.4 wt % is in good agreement with the ratio of the products obtained in reaction 7, considering that the decomposition temperature of LiH is much higher than 200 °C.³⁴ It may also be noted that at 200 °C Li_3AlH_6 releases only 1.5 mole of H_2 gas (50 % of the total hydrogen content by weight) according to reaction 11 below.

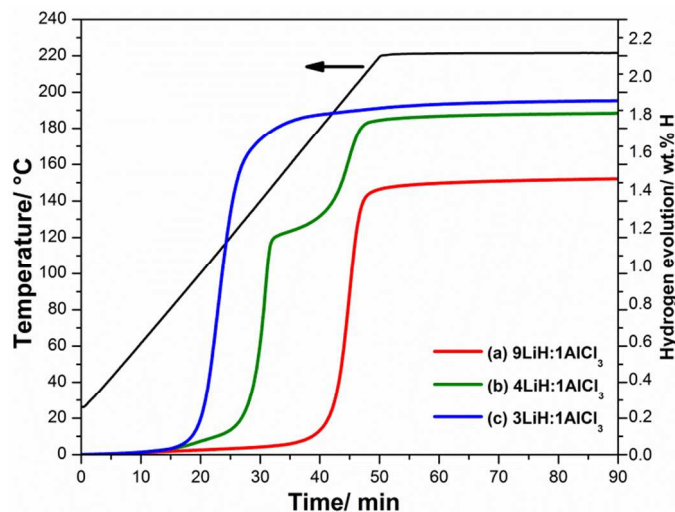
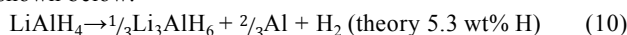


Fig. 5 TPD curves obtained for samples of the reaction mixtures resulting from LiH:AlCl₃ starting ratios of a) 9:1, b) 4:1, and c) 3:1 after 48 min of ball-milling under 350 bar H₂ with a milling speed of 300 rpm and a b:p of ~140. Note that these samples correspond (respectively) to the final products obtained upon completion of the first, second, and final stages of the stepwise mechanochemical synthesis of alane, as described in the text and shown in Eqs 7, 8, and 9.

The curve (b) in Fig. 5 represents the decomposition profile of the products obtained after the second stage (Eq. 8). The two-step decomposition with T_d 's close to 130 °C and 180 °C is in excellent agreement with the decomposition pathway of LiAlH_4 as shown below.³⁴



The measured hydrogen capacity of ca. 1.8 wt % also agrees well with the theoretical value of 1.87 wt %, assuming that the reaction 8 proceeds to completion. Finally, the desorption profile of the products from reaction 9 shows a one-step decomposition with a T_d of ca. 90 °C, as typically expected for AlH_3 ,³⁶ and the net hydrogen evolution corresponding to 1.9 wt %, which confirms the completion of the reaction. In all three cases, mass-spectroscopic analyses showed that H₂

constituted 99.7 % or more of the gases released, the rest being residual air. The XRD analyses of desorbed samples from the 9:1 and 4:1 mixtures showed Bragg peaks corresponding to metallic Al, LiH and LiCl. On the other hand only metallic Al and LiCl were observed in the desorbed 3:1 sample, which suggests that LiH was completely consumed during the mechanochemical processing and that all of the alanes formed as intermediates during the first two stages were transformed to alane (Fig. S5†). To summarize, the desorption profiles of the products obtained after stages 1–3 are in excellent agreement with the XRD and SSNMR analyses, and thereby further validate the suggested pathway for this mechanochemical transformation, as given by Eqs. 7-9.

3.7 Reaction mechanisms

To explain why the reaction between LiH and AlCl₃ in a 3:1 molar ratio leads to metallic Al even under H₂ pressure, products from this reaction were analysed for $\tau_{\text{BM}} = 6, 12$ and 18 min. It was observed that the 3:1 reaction does not yield metallic Al right away, but rather proceeds to form a small amount of LiAlCl₄ at $\tau_{\text{BM}} = 18$ min, a pathway similar to that of the 9:1 reaction. (Caution! this product, which likely contains AlCl₂H and AlClH₂, is highly unstable and reacts vigorously under argon even upon a slight impact to yield metallic Al and H₂ gas). However, in contrast to 9:1 reaction after 18 min, a significant amount of unreacted AlCl₃ was also noticed in the 3:1 mixture, which suggests that the 3:1 reaction is slower under similar milling conditions. A comparison of the progress of 3:1 and 9:1 reactions within the first 20 min of milling is shown in Fig S6†. Whereas the formation of Li₃AlH₆ is already evident in the 9:1 mixture for $\tau_{\text{BM}} = 24$ min, no alane peaks are observed in the 3:1 reaction. Thus, one may infer that in the presence of excess LiH in the mixture, the formed intermediates (likely a mixture of AlCl₂H and AlClH₂) are readily transformed to alane before decomposing into metallic Al. In parallel to the observations made by Mikheeva *et al.* during their studies of the reaction between LiH and AlCl₃ (in ether), the following argument may explain to some extent the failure of the stoichiometric 3:1 and 4:1 reactions.³⁷ Because of its relatively low volume fraction in these mixtures compared to 9:1, LiH may not be sufficiently dispersed, leading to high local AlCl₃/LiH ratios. This in turn may lead to the decomposition of unstable chlorine-containing derivatives such as AlCl₂H and AlClH₂ (or AlH₃AlCl₃) into metallic Al with evolution of hydrogen, rather than the formation of alane. It was also noticed by Mikheeva *et al.* that slow addition of an ethereal solution of AlCl₃ improved the yield of LiAlH₄, which is akin to the required sequential addition of AlCl₃ in the present case.

To obtain further insight, another reaction was performed in which the 3:1 LiH:AlCl₃ reaction mixture was processed at half the milling speed (150 rpm) and, as before, at 350 bar H₂ pressure. It was observed that the reaction progresses without the formation of metallic Al, albeit at a very slow pace, so much so that it was incomplete even after 20 h of milling, as shown by SSNMR results (Fig S7†). More interestingly, this latter reaction could also be performed at a relatively low H₂ pressure of less than 10 bar, although the reaction time remained unaffected. However, when this reaction was performed under argon at a pressure slightly over 1 bar (*i.e.*, glove box pressure), metallic Al was obtained within 60 min of milling. Based on these results one may naively conclude that at low milling speeds the local temperature spikes are insignificant when compared to those at high milling speeds, which prevents the decomposition of AlH₃. However there may be two caveats to

this view. First, it is well known that AlH_3 is kinetically metastable at room temperature with equilibrium pressure of $>1\text{GPa}$. It is quite unlikely in this scenario that a moderate gas pressure of 350 bar could prevent the decomposition of nascent AlH_3 . Second, this view does not support the formation of metallic Al in the 4:1 mixture since it would only lead to LiAlH_4 as a final product (Eq. 3), which is known to be stable under milling unless carried out in the presence of a catalyst such as titanium.³⁸ It is quite intriguing to note that the 9:1 composition, which is far from the equilibrium composition of 3:1, still requires a pressure of about 300 bar to prevent the formation of metallic Al at 300 rpm. Although the minimum pressures required during the second and third stages were not determined independently in this work, it is known that a certain critical pressure (ca. 200 bar) is needed to prevent the formation of metallic Al during the reaction given by Eq. 9.³⁹ Although the role of pressure during processing is not clearly understood, it is postulated that the gas under pressure acts as a fluid medium that may assist in the long-range solid-state diffusion of ions that is essential for preventing the destabilization of Al-H bonds. Alternatively, it is also likely that the high-pressure gas may serve as an effective heat transport medium and hence alter the mechanochemical reaction pathway.

It is also clear that manipulation of the gas pressure alone may not be sufficient to avoid the Al-H decomposition pathway. Indeed, the minimum required pressure for the 9:1 reaction is 300 bar, whereas the minimum for the 3:1 reaction (if any) is higher (likely, much higher) than 350 bar. Thus, the presence of excess LiH in the mixture appears to be essential for the preservation of the newly formed Al-H bonds *via* the formation of intermediate, thermodynamically stable alanates.

4. Conclusion

A solvent-free mechanochemical route has been developed for the preparation of alane starting from LiH and AlCl_3 at room temperature. Although this reaction has been known to occur in solvents such as diethyl ether, it is important to discover methods that are simple to carry out on a large scale. In contrast to the wet-chemical route however, the direct solvent-free mechanochemical reaction of LiH and AlCl_3 at a ratio of 3:1 or 4:1 fails to yield AlH_3 or LiAlH_4 , respectively. Instead, the use of excess LiH in the starting mixture leads to conditions that favour the formation of Al-H bonds resulting in the intermediate alanates. The results described in this work establish this mechanochemical route as a versatile and very useful alternative to solution-based methods, which reduces or eliminates the use of potentially hazardous solvents. We note, however, that in addition to non-solvated alane, the resulting material contains about 80% of dead weight in the form of LiCl by-product, which reduces the net gravimetric hydrogen density by the same amount. Separation of alane from LiCl is thus critical for realizing its full potential as a hydrogen storage material. Although different solubilities of alane and LiCl in various organic solvents have been employed with varying success to achieve the separation, future research must focus on finding a suitable solvent, or a combination of solvents, that are both inexpensive and benign. Other separation techniques (including solvent-free) may become practical if similar reactions are performed using different starting hydrides and/or aluminium salts leading to more easily separable by-product. It is also demonstrated that the mechanochemical reaction pathway can be altered by adjusting the applied gas pressure. In the present

case, this was demonstrated by manipulating the H₂ pressure such that the reaction pathway leading to metallic Al was completely avoided. Although the exact role of the gas pressure could not be clearly elucidated, it is postulated that the gas under high pressure acts as a fluid medium, which may have significant effects on the underlying solid-state diffusion processes. Alternatively, the high-pressure gas may serve as an effective heat transfer medium, which may alter the local temperature profile and thereby affect the reaction pathway. The ability to successfully synthesize alane at room temperature also eliminates the need for cryogenic cooling to suppress the formation of metallic Al. A better understanding of the mechanistic pathway for the synthesis of alane is expected to provide the much needed basic scientific insight necessary for the development of more refined approaches not only toward production of AlH₃, but also related reactions, including the direct mechanochemical hydrogenation of metallic Al, which remains elusive to this day.

Acknowledgements

This work was supported by the U.S. Department of Energy (DOE), Office of Science, Basic Energy Sciences, Materials Science and Engineering Division. The research was performed at the Ames Laboratory, which is operated for the U.S. DOE by Iowa State University under contract No. DE-AC02-07CH11358.

References

- ^a Ames Laboratory, Iowa State University, Ames, IA 500011-3020, USA. FAX: 515 294 9579; Tel: 515 294 9158; E-mail: shalabh@ameslab.gov
- ^b Department of Chemistry, Iowa State University, Ames, IA 500011-3111, USA. FAX: 515 294 4709; Tel: 515 294 2017; E-mail: mpruski@iastate.edu
- ^c Department of Materials Science and Engineering, Iowa State University, Ames, IA 50011-2300, USA. FAX: 515 294 9579; Tel: 515 294 8220; E-mail: vitek@ameslab.gov
- † Electronic Supplementary Information (ESI) available: ²⁷Al DPMAS reference spectra for LiAlCl₄, LiAlH₄, AlCl₃, and Al₂O₃; Integrated peak intensities obtained from the ²⁷Al DPMAS spectra collected for Stages 1-3; ²⁷Al 5QMAS spectra obtained for LiAlCl₄ and LiAlH₄; XRD patterns of products obtained after TPD; XRD patterns comparing the progress of the 3:1 and 9:1 reaction mixtures during the first 20 min of milling; ²⁷Al DPMAS and ²⁷Al{¹H} CPMAS spectra for a 3:1 LiH:AlCl₃ sample milled for 20 h at 150 rpm under 350 bar H₂. See DOI: 10.1039/b000000x/.
1. L. Schlapbach and A. Züttel, *Nature*, 2001, **414**, 353.
 2. D. Abbott, *Proceedings of the IEEE*, 2010, **98**, 42.
 3. J. Graetz, J. Reilly, V. Yartys, J. Maehlen, B. Bulychev, V. Antonov, B. Tarasov and I. Gabis, *J. Alloys Compd.*, 2011, **509**, 517.
 4. http://www1.eere.energy.gov/hydrogenandfuelcells/storage/pdfs/targets_onboard_hydro_storage_explanation.pdf
 5. J. M. Pasini, C. Corgnale, B. A. van Hassel, T. Motyka, S. Kumar and K.L. Simmons, *Int. J. Hydrogen Energy*, 2013, **38**, 9755.
 6. O. Stecher, E. Wiberg, *Ber. Dtsch. Chem. Ges.*, 1942, **75B**, 2003.
 7. A.E. Finholt, A.C. Bond and H.I. Schlesinger, *J. Am. Chem. Soc.*, 1947, **69**, 1199.
 8. G. Chizinsky, *J. Am. Chem. Soc.*, 1955, **77**, 3164.
 9. F. Brower, N. Matzek, P. Reigler, H. Rinn, C. Roberts, D. Schmidt, J. Snover and K. Terada, *J. Am. Chem. Soc.*, 1976, **98**, 2450.
 10. C. Ashby, J.R. Sanders, P. Claudy and R. Schwartz, *J. Am. Chem. Soc.*, 1973, **95**, 6485.

11. A.E. Finholt, G.D. Barbaras, G.K. Barbaras, G. Urry, T. Wartik and H.I. Schlesinger, *J. Inorg. Nucl. Chem.*, 1955, **1**, 317.
12. B. M. Bulychev, A. V. Golubeva, P. A. Storozhenko, *Russ. J. Inorg. Chem.*, 1998, **43**, 1765.
13. S.K. Konovalov and B.M. Bulychev, *Inorg. Chem.*, 1995, **34**, 172.
- 5 14. J. Graetz, *Chem. Soc. Rev.*, 2009, **38**, 73.
15. R. Zidan, B.L. Garcia-Diaz, C.S. Fewox, A.C. Stowe, J.R. Gray and A.G. Harter, *Chem. Comm.*, 2009, **25**, 3717.
16. G.S. McGrady, US Patent US 2008/0241056 A1, 2 October, 2008.
17. L.V. Dinh, D. A. Knight, M. Paskevicius, C.E. Buckley and R. Zidan, *Appl. Phys. A*, 2012,
10 **107**, 173.
18. H.W. Brinks, A. Istad-Lem and B.C. Hauback, *J. Phys. Chem. B*, 2006, **110**, 25833.
19. M. Paskevicius, D.A. Sheppard and C.E. Buckley, *J. Alloys Compd.*, 2009, **487**, 370.
20. Y.C. Luo, S. K. Mao, R. X. Yan, L. B. Kong and L. Kang, *Acta Physico-Chimica Sinica*,
2009, **25**, 237.
- 15 21. E.C. Ashby, G.J. Brendel and H.E. Redman, *Inorg. Chem.*, 1963, **2**, 499.
22. N.N. Mal'tseva, K.G. Myakishev, A.I. Golovanova, V.V. Volkov and N. Kuznetsov, *Zh. Neorg. Khim.*, 1989, **34**, 40.
23. A.E. Bennett, C.M. Rienstra, M. Auger, K.V. Lakshmi, R.G. Griffin, *J. Chem. Phys.* 1995,
103, 6951.
- 20 24. PDF 74-1972 (ICDD, 2000).
25. PDF 70-435 (ICDD, 2000).
26. G. Mairesse, P. Barbier, J. P. Wignacourt and P. Baert, *Cryst. Struct. Commun.*, 1977, **6**, 15.
27. PDF 78-839 (ICDD, 2000).
28. E. Wiberg, M. Schmidt, H. Graf, and R.U. Lacial, *Z. Naturforsch.*, 1952, **7b**, 578.
- 25 29. E. Wiberg, M. Schmidt, *Z. Naturforsch.*, 1951, **6b**, 333.
30. G. Sandrock, J. Reilly, J. Graetz, W.-M. Zhou, J. Johnson and J. Wegrzyn, *J. Alloys Compd.*,
2006, **421**, 185.
31. PDF 73-461 (ICDD, 2000).
32. PDF 27-282 (ICDD, 2000).
- 30 33. I. Zaluski, A. Zaluska and J. O. Storm-Olsen, *J. Alloys Compd.*, 1999, **290**, 71.
34. J.A. Dilts and E.C. Ashby, *Inorg. Chem.*, 1972, **11**, 1230.
35. V.P. Balema, V.K. Pecharsky and K.W. Dennis, *J. Alloys Compd.*, 2000, **313**, 69.
36. G. Sandrock, J. Reilly, J. Graetz, W.-M. Zhou, J. Johnson and J. Wegrzyn, *Appl. Phys. A*,
2005, **80**, 687.
- 35 37. V.I. Mikheeva, E.M. Fedneva and Z.L. Shnitkova, *Zh. Neorg. Khim.*, 1956, **1**, 2440.
38. V. P. Balema, J. W. Wiench, K. W. Dennis, M. Pruski and V. K. Pecharsky, *J. Alloys
Compd.*, 2001, **329**, 108.
39. S. Gupta, T. Kobayashi, I.Z. Hlova, M. Pruski and V.K. Pecharsky, unpublished.